

See discussions, stats, and author profiles for this publication at: <https://www.researchgate.net/publication/49813552>

Modelling millimetre wave propagation and absorption in a high resolution skin model: The effect of sweat glands

Article in *Physics in Medicine and Biology* · March 2011

DOI: 10.1088/0031-9155/56/5/007 · Source: PubMed

CITATIONS

24

READS

180

2 authors:



Gal Shafirstein

Roswell Park Cancer Institute

98 PUBLICATIONS 948 CITATIONS

[SEE PROFILE](#)



Eduardo G Moros

H. Lee Moffitt Cancer Center and Research Institute

377 PUBLICATIONS 4,082 CITATIONS

[SEE PROFILE](#)

Some of the authors of this publication are also working on these related projects:



PET Research in Radiation Oncology [View project](#)



FORT- The Future of Radiation Therapy [View project](#)

Modelling millimetre wave propagation and absorption in a high resolution skin model: the effect of sweat glands

This article has been downloaded from IOPscience. Please scroll down to see the full text article.

2011 Phys. Med. Biol. 56 1329

(<http://iopscience.iop.org/0031-9155/56/5/007>)

View [the table of contents for this issue](#), or go to the [journal homepage](#) for more

Download details:

IP Address: 138.26.16.5

The article was downloaded on 07/03/2011 at 05:34

Please note that [terms and conditions apply](#).

Modelling millimetre wave propagation and absorption in a high resolution skin model: the effect of sweat glands

Gal Shafirstein¹ and Eduardo G Moros²

¹ Department of Otolaryngology, College of Medicine, University of Arkansas for Medical Sciences, 4301 W. Markham, # 543, Little Rock, AR 72205, USA

² Division of Radiation Physics and Informatics, Department of Radiation Oncology, College of Medicine, University of Arkansas for Medical Sciences, 4301 W. Markham, #771, Little Rock, AR 72205, USA

E-mail: shafirsteingal@uams.edu

Received 15 September 2010, in final form 6 January 2011

Published 4 February 2011

Online at stacks.iop.org/PMB/56/1329

Abstract

The aim of this work was to investigate the potential effect of sweat gland ducts (SGD) on specific absorption rate (SAR) and temperature distributions during mm-wave irradiation. High resolution electromagnetic and bio-heat transfer models of human skin with SGD were developed using a commercially available simulation software package (SEMCAD XTM). The skin model consisted of a 30 μm stratum corneum, 350 μm epidermis and papillary dermis (EPD) and 1000 μm dermis. Five SGD of 60 μm radius and 300 μm height were embedded linearly with 370 μm separation. A WR-10 waveguide positioned 20 μm from the skin surface and delivering 94 GHz electromagnetic radiation was included in the model. Saline conductivity was assigned inside SGD. SAR and temperatures were computed with and without SGD. Despite their small scale, SAR was significantly higher within SGD than in the EPD without SGD. Without SGD, SAR and temperature maxima were in the dermis near EPD. With SGD, SAR maximum was inside SGD while temperature maximum moved to the EPD/stratum-corneum junction. Since the EPD participates actively in perception, the effect of SGD should be taken into account in nociceptive studies involving mm-waves. This research represents a significant step towards higher spatial resolution numerical modelling of the skin and shows that microstructures can play a significant role in mm-wave absorption and induced temperature distributions.

1. Introduction

The last 20 years have witnessed an explosion in human exposure to electromagnetic (EM) radiation in the millimetre-wave band. When aimed towards humans, radiation in this part of the EM spectrum is mostly absorbed in the skin (Alekseev *et al* 2005, 2008, Alekseev and Ziskin 2003, 2007, Walters *et al* 2000). The interaction of millimetre wave (mm-wave) radiation with the skin depends on the dielectric properties of the various components of the skin. It is well known that dielectric properties of biological tissues substantially depend on water content (Alekseev *et al* 2008, Naito *et al* 1997). The dielectric properties of the human skin *in vivo* in the range of the frequencies of 37–74 GHz under the assumption that the dielectric constant of the various skin layers is determined by their respective bulk water content was investigated by Alekseev *et al* (2008) and Alekseev and Ziskin (2007). They also assumed that the non-constitutive water contained in the stratum corneum (SC) affects the interaction of mm-wave with human skin. In their model, the skin structure was described as two layers: the SC and a combined epidermis and papillary dermis (EPD)/dermis layer. Analytical and finite differences methods were used to model EM propagation, reflection and absorption in the skin in the forearm and palm of the hand. The thickness of the SC was assumed to be 0.015 and 0.4 mm in the forearm and palm, respectively, and the modelling was verified with experimental results. Their work showed that the thicker the SC (more water) the more reduced was the reflection of the mm-wave radiation. A thick and moist SC acted as a matching layer (Alekseev *et al* 2008).

Recent studies by Feldman *et al* (2008), (2009) suggested that the human eccrine sweat ducts or sweat gland ducts (SGD) have a major effect on the reflection and propagation of mm-waves in the human skin. The eccrine sweat duct system is responsible for thermoregulation of the body and is under the control of the sympathetic nerve response (Shibasaki *et al* 2006). The EPD contains between 2 and 5 million SGD that extend into the dermis. The concentration of these glands varies from site to site in the human body (Wilke *et al* 2007). The greatest density of SGD is on the palms of the hands and soles of the feet, followed by the head, trunk and limbs. Increased sweating occurs through the combination of increasing the number of sweat glands that are activated and increasing the amount of sweat released per gland. Sweat is primarily water (99%) and therefore it can influence the absorption of mm-waves in skin. Furthermore, the shape of the sweat glands can also affect the absorption and reflection of mm-waves by the skin. Feldman *et al* (2008), (2009) demonstrated that the helical part of the SGD located in the EPD may act as low Q helical antennas. They have shown that for the frequency region of 75–110 GHz (within the W band) the helical glands will affect the modulus of reflection. They assumed that proton hopping was the primary mechanism for electrical current transport along the sweat ducts during exposure to mm-wave radiation. They verified their results with a clinical study. Thus, their work offers a new direction in the understanding of the absorption of mm-waves in the human skin. However, in their studies, the effect of the SGD on the specific absorption rate (SAR) and resulting temperature increase was not investigated. The objective of this work was to model the effect of SGD on SAR and temperature increase due to exposure of skin with SGD to mm-wave radiation.

2. Methods

2.1. Electromagnetic modelling

The SEMCAD X (Schmid & Partner Engineering AG, Zurich, Switzerland) finite differences time domain (FDTD) software was used to simulate the propagation and interactions of 94 GHz

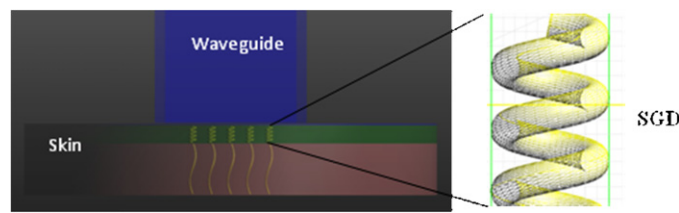


Figure 1. Cross section of the waveguide (blue) and the skin geometry (green and brown) showing the SGD (yellow) embedded in the EPD and dermis. A conformal elongated grid was used to mesh the SGD. The green grid in the background is the mesh in the EPD region.

electromagnetic (EM) radiation in a three-dimensional numerical model of the skin containing a few SGD. A cylinder of 8 mm in diameter and 1.38 mm high was used to simulate the skin anatomy. The cylinder consisted of a 0.03 mm upper layer representing the SC, a 0.35 mm intermediate layer representing EPD, and a 1 mm thick dermis at the base. Five SGD of helical shape were embedded linearly, with 370 μm separations, within the EPD and extended into the dermis (figure 1).

Each helix (SGD) was 0.3 mm high and 0.12 mm in diameter. The sweat ducts themselves were 0.04 mm in diameter coiled into four equally spaced turns. The rectangular waveguide (WR-10) was modelled to deliver 94 GHz EM radiation, 3.21 mm wavelength in air, to the skin model. The waveguide, 14 mm long with 2.45 mm \times 1.27 mm dimensions, was located at the centre of the skin disc. An EM source was placed 13.6 mm away from the mouth of the waveguide to generate EM waves propagating in a TE₁₀ mode towards the waveguide's mouth, which was positioned 0.02 mm from the surface of the SC. The entire model was encompassed within a geometrical box (bounding box) with padding of 0.25 of the maximum wavelength on all side. The bounding box bounds the volume in which the EM radiation was allowed to propagate. The properties of the space between the faces of the box and the skin and waveguide geometries, were those of air. Uniaxial perfectly matched layers boundary conditions were applied to the bounding box faces. Medium boundary strength (>95% absorption) was specified on all the sidewalls of the bounding box and high absorption (>99% absorption) was set for the top and bottom faces of the box, above the waveguide and below the skin model. A progressive grid with 2.645×10^6 voxels was used to mesh the entire geometry (skin and waveguide). The overall grid size was determined by refining it to the point where any further refinements resulted in changes of no more than 5% in the results. Thus, the accuracy of the simulation is $\pm 5\%$. Within the geometrical model the minimum steps of the grid were 1.5×10^{-5} m (15 μm) in the X and Y directions and 10^{-5} m (10 μm) in the Z direction. Using analytic modelling presented elsewhere (Pickard and Moros 2001) it can be shown that for a forward travelling 94 GHz plane wave, the wavelength is 1.15 mm in a biological tissue with relative permittivity of 5.8 and conductivity of 39 S m⁻¹. Therefore, the maximum grid size was 0.1 mm which is less than 1/10 of the wavelength. The glands were meshed with a conformal triangular grid with 10^{-6} m resolution (1 μm) as shown in figure 1. There were 436 voxels in each SGD and 221 in each of the SGD extensions.

A forward power of 30 mW that translates to 9.3 kW m⁻² was delivered from the waveguide towards the skin. The EM properties for each skin constituent at 94 GHz that were used are listed in table 1. These properties were calculated using Gabriel and Gabriel empirical equation and data (Gabriel *et al* 1996a, 1996b, 1996c), which are included in the SEMCAD software. The EM properties of the content inside the sweat glands were assumed to be those of saline (at 94 GHz) and were taken from Pickard *et al* (2010). Note, that the ac conductivity

Table 1. Electromagnetic and thermal properties of the various skin structures used in the model.^a

Region	Conductivity (S m ⁻¹)	Relative permittivity	Density (kg m ⁻³)	Thermal conductivity (W m ⁻¹ C ⁻¹)	Specific heat capacity (J kg ⁻¹ C ⁻¹)	Blood perfusion (m _b ³ /m _t ³ /s)
Dermis	39	5.8	1100	0.35	3437	1.78 × 10 ⁻³
EPD	1	3.2	1200	0.21	3600	none
Stratum corneum	0.0001	2.4	1000	0.21	3600	none
Gland	83	3.9	1000	0.53	4190	none

^a The relative permeability was 1 for all regions.

of the SGD (83 S m⁻¹) is close to the maximum value (100 S m⁻¹) measured in water for proton hopping (Cukierman 2000). The SAR distribution was calculated for two cases: (1) equating the SGD properties to the EPD and dermis (i.e. effectively having no glands) and (2) setting the glands properties equal to saline's properties. The exact same geometry and grid were used in both cases. The transient EM simulation was conducted until it reached steady state.

Noteworthy, Johnsen *et al* (2010) found that the water content in the SC is 0.076–0.0863 mg cm⁻² under normal conditions. That is about 2.59×10^{-3} mg cm⁻³ which represents an extremely low volume fraction. Thus, from a practical point of view the SC can be considered as nonconductive layer, as assumed by Feldman *et al* (2009) and Alekseev *et al* (2008) in this study.

2.2. Thermal modelling

The temperature increase due to the EM radiation was computed by importing the calculated three-dimensional SAR field into the bio-thermal solver module of SEMCAD. The same skin geometry and grid that were used for the EM simulations were used in the thermal simulations. The heat source (W m⁻³) in each voxel of the thermal simulation was created by multiplying the SAR (W kg⁻¹) by the specific density (kg m⁻³) of the respective tissue in each voxel. The thermal property values were assumed to be independent of the EM field and were taken from Shafirstein *et al* (2004). The initial condition for the temperature (T) was 32 °C following Alekseev and Ziskin (2003). Dirichlet boundary conditions ($T = 32$ °C) were applied to the bottom of the skin cylinder and the circumferential cylinder wall. The boundary condition on the top surface of the cylinder, the surface of the SC facing the waveguide, was

$$-k\nabla T|_{z=0,x,y} = h(T - T_{\text{ext}}). \quad (1)$$

T_{ext} was set to 26 °C and the convection coefficient h was set to 15 W C⁻¹ m⁻², assuming slow air flow over a flat plate (Holman 1981). Blood perfusion of 1.78×10^{-3} m_b³ m_t⁻³ s⁻¹ was set in the dermis with arterial blood temperature of 36 °C. The transient thermal simulations were run until steady state was reached, usually about 20 s.

3. Results

The EM simulation reached a steady state in 20 cycles. The SAR distribution for no SGD (case 1) is shown in figure 2, which plots the x - z plane, through the middle of the skin model (no SDG).

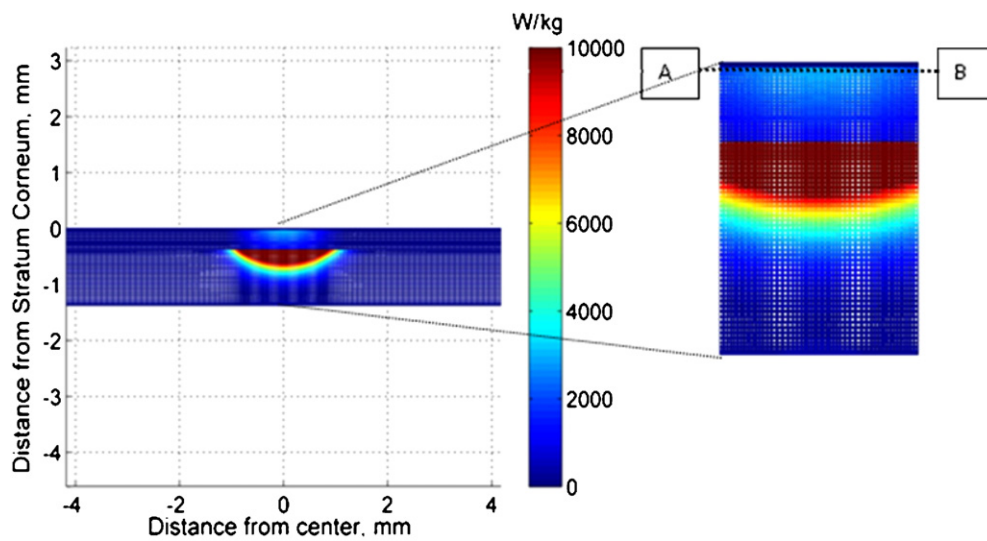


Figure 2. Cross section of the 94 GHz irradiation induced SAR distribution. The A–B line is the depth at which the SAR distribution was plotted along the distance from the centre in figure 5.

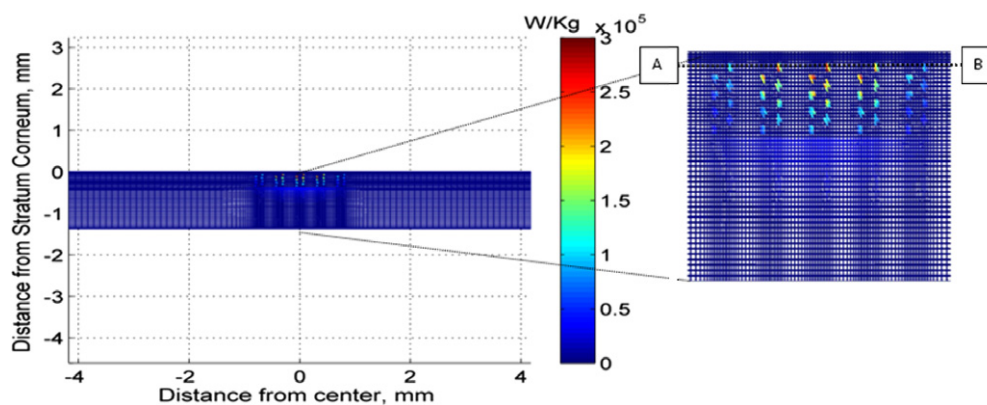


Figure 3. Cross section of the 94 GHz irradiation induced SAR distribution with SGD. The A–B line is the depth at which the SAR distribution was plotted along the distance from the centre in figure 5.

Figure 3 shows the calculated SAR distribution through the middle of the skin model, bisecting the SGD. Maximum SAR of $288\,000\text{ W kg}^{-1}$ (see figure 5) was calculated at the upper coil of SGD embedded in the EPD.

In figure 4 we present the SAR profile as a function of distance from the surface, for the case of no SGD. The SAR is minimal at the SC layer, due to the very low conductivity of this skin constituent (it was assumed to be dry). Maximum SAR values of 2494 W kg^{-1} and $32\,500\text{ W kg}^{-1}$ were calculated in the EPD and dermis, respectively. Within the EPD, with no SGD, the SAR decreases as a function of depth due to the attenuation of the electric field (E-field). However, a rapid increase in the SAR is seen at the epidermal/dermal junction (figure 4). This increase is due to the relatively high electrical conductivity of the dermis in

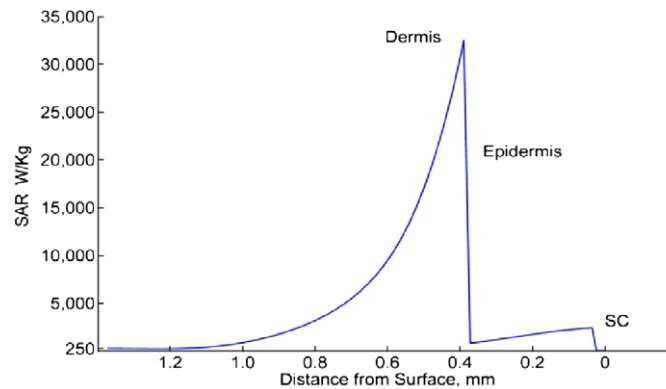


Figure 4. The SAR distribution as a function of distance from the surface of the skin with no SGD.

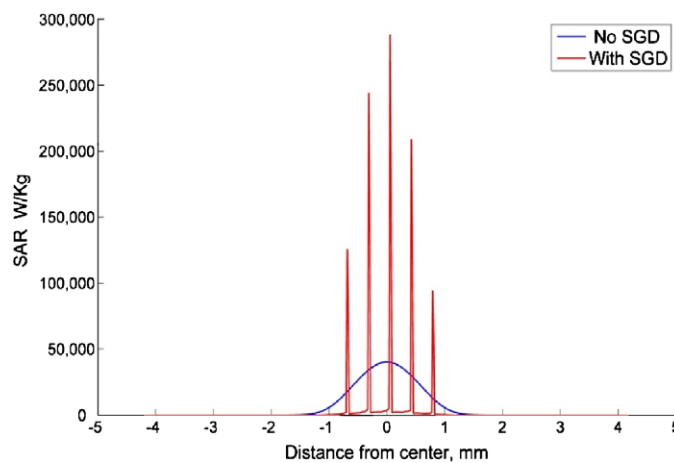


Figure 5. The SAR distribution along the line A–B as shown in figures 2 and 4 for the geometry with no SGD and with SGD.

comparison to the EPD, i.e. 39 S m^{-1} versus 1 S m^{-1} . Within the dermis, the SAR decays from $32\,500 \text{ W kg}^{-1}$ to 255 W kg^{-1} (figure 4) due to the E-field attenuation in the dermis.

The effect of the SGD on the SAR is clearly seen in figure 5 where the SAR linear distribution bisecting the SGD is plotted at depth of $100 \mu\text{m}$ from the top surface (along line A–B in figures 2 and 3). A maximum SAR of $288\,000 \text{ W kg}^{-1}$ was calculated within the central SGD. The SAR in the adjacent SGD was slightly lower, due to the E-field distribution in reference to the centre of the waveguide and geometry. The SAR inside the SGD with saline was about one order of magnitude higher than the SAR at the same location but with properties of the embedding tissue.

The resulting temperature distributions, for the SAR shown in figures 2 and 3, are shown in figure 6.

It can be clearly seen that the presence of the SGD resulted in an increase of temperature within the EPD towards the SC (figures 6(A) versus (B)). At the EPD/SC junction the temperature increase was 5.9°C and 6.9°C for cases 1 and 2, respectively (figure 7(A)). Near

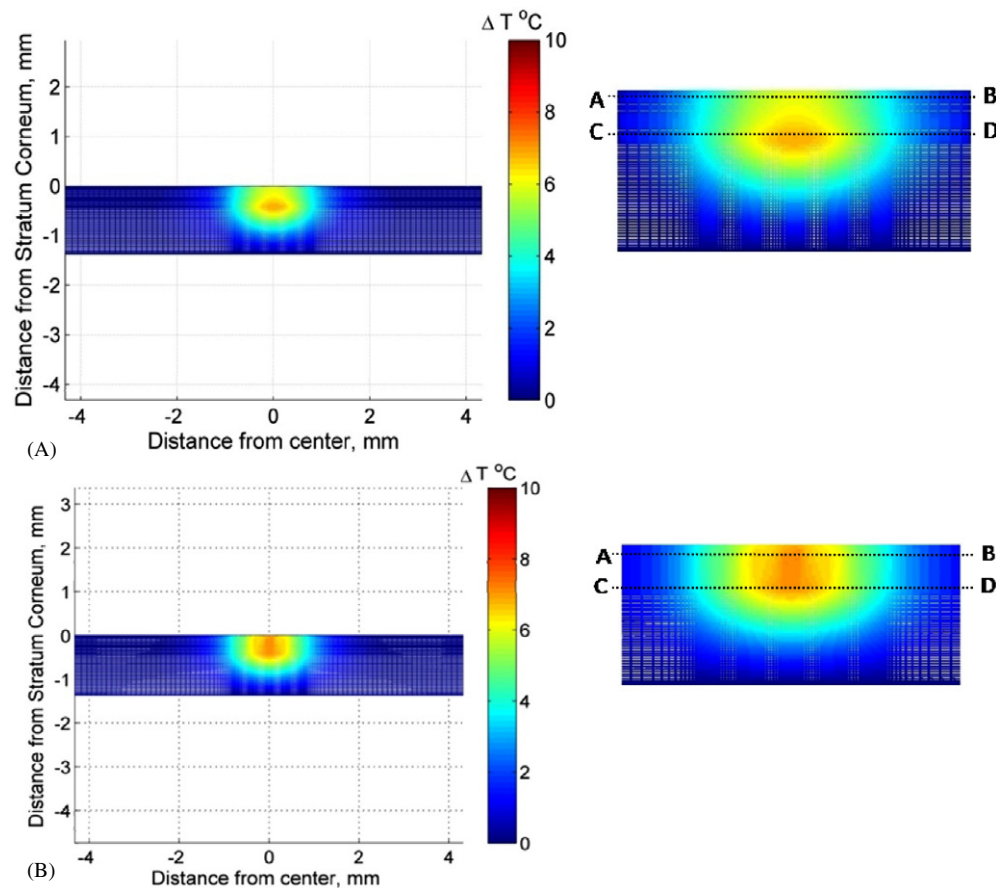


Figure 6. The temperature distribution within a cross section of the skin geometry with no SGD (A) and with SGD (B). The lines A–B and C–D indicate the depths of which the temperature distributions were plotted against the distance from the centre in figure 7.

the epidermal/dermal junction the maximum temperature increase was 6.8°C and 7.3°C for cases 1 and 2, respectively (figure 7(B)). A steady state temperature increase was achieved in 20 s in both cases (figure 8).

The maximum temperature difference between the two cases was less than 0.5°C at, steady state, $t > 20$ s (figure 8).

4. Discussion

In this work, we investigated the effect of helical SGD on SAR and temperature distribution during 94 GHz irradiation of skin. The simulations employed a geometry of the skin and SDG that is similar to the one presented by Feldman *et al* (2009). Unlike Feldman *et al*, however, we assumed that the conductivity of the content of the SGD (i.e. sweat) was similar to saline, 83 S m^{-1} at 94 GHz, according to our previous work (Pickard *et al* 2010). Our results are in general agreement with the theoretical analysis and clinical measurements of Feldman *et al* (2009). The simulations clearly show that SGD act as high absorption sites for mm-wave

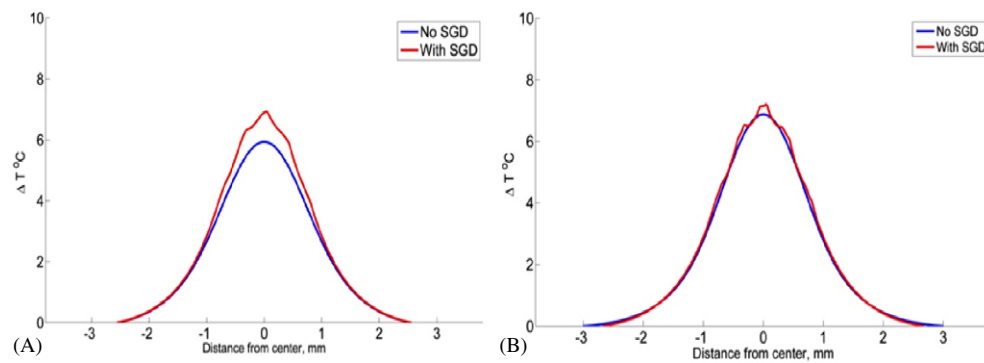


Figure 7. (A) The steady state temperature distribution along line A–B at the EPD/SC junction (see figure 6) and (B) along line C–D, in figure 6, at the EPD/dermis junction.

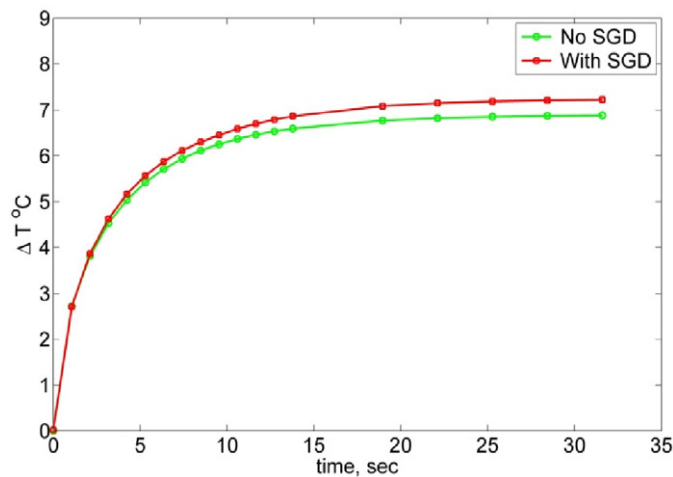


Figure 8. The maximum temperature increase as a function of time at the EPD/dermis junction for the geometries with and without SGD.

radiation (figure 3). A maximum SAR of $288\,000\text{ W kg}^{-1}$ was calculated within the glands versus maximum SAR of 2494 W kg^{-1} within the EPD with no SGD (figures 2 and 5). In our previous work we showed that a maximum SAR of 4500 W kg^{-1} induced a temperature increase of $0.5\text{ }^{\circ}\text{C}$ inside a small chamber containing cells (Pickard *et al* 2010). Assuming a linear relationship between SAR and steady state temperature increase, a maximum temperature increase of about $32\text{ }^{\circ}\text{C}$ within the centre SGD would be expected. However, the calculated maximum temperature increase was only $7\text{ }^{\circ}\text{C}$ (figure 8). This discrepancy can be explained by careful examination of the model. In the EM simulation the high SAR ($288\,000\text{ W kg}^{-1}$) was extremely local ($<0.01^3\text{ mm}^3$) at the tip of the gland which included only a few voxels. In the thermal simulation these few voxels represented a very small heat source ($\sim 10^{-6}\text{ mm}^3$) with extremely high surface area to volume ratio that induced rapid heat dissipation, thereby resulting in a lower temperature increase when compared to the results of Pickard *et al* (2010).

A steady state temperature was reached after about 20 s of continuous exposure to the 94 GHz irradiation (figure 8). This is a longer time in comparison to the results presented in Pickard *et al* (2010) where thermal equilibrium was obtained after 10 s. However, in that work the overall radiated volume was smaller and the heating was more uniform (without the SAR spikes due to SGD) than the present one. In addition, the rate of heat dissipation to the ambient air by convection was much higher ($h = 750 \text{ W m}^{-2} \text{ C}^{-1}$ versus $15 \text{ W m}^{-2} \text{ C}^{-1}$). These two effects explain the shorter time required to reach thermal equilibration in Pickard *et al* (2010).

The calculated maximum temperature, in this work, is in agreement with temperature increase measured in skin of healthy volunteers exposed to 94 GHz radiation (Walters *et al* 2000). In that human study, a skin temperature rise of roughly 10°C was measured after a 3 s exposure to 18 kW m^{-2} at 94 GHz radiation. In our simulation, a temperature increase of about 4.5°C (figure 8) was calculated for a 3 s exposure at 9.3 kW m^{-2} of 94 GHz radiation. Assuming a linear relationship between the temperature increase and the forward power, it can be concluded that our predicted temperature increase is in agreement with the measurements reported in Walters *et al* (2000).

Our results also suggest that the majority of the mm-wave radiation is absorbed in the EPD and upper dermis while the SC does not contribute to the temperature increase. This result is not in full agreement with the analysis of Alekseev *et al* (2008), who calculated the SARs in response to mm-wave radiation (at 42 and 61 GHz) in the skin of the forearm and palm of hands. They assumed that the amount of free water in the SC is the key parameter that affects the reflection of the EM waves from the palm and forearm. They postulated that the differences in SAR between the forearm and the palm was due to the difference in the thickness of the SC, 0.015 versus 0.42 mm for forearm and palm, respectively (Alekseev *et al* 2008). Thus, thicker SC translates to higher water content and higher absorption in the palm in comparison to the forearm. We posit that the differences in the SARs between the palm and the forearm are due to the differences in the density of SGD in these regions (Wilke *et al* 2007). Sweat gland density in the palm is about five times the density in the forearm (644 versus 134 SGD per cm^2) (Wilke *et al* 2007). Our results suggest that an increase in number of SGD would result in higher average SAR. Sweat is about 99% water and 1% salt and amino acids; hence, it is plausible that the increase of sweat gland density in the palm will result in a more hydrated SC that will affect the reflection of the EM waves, as observed by Alekseev *et al* (2008). In this sense, our results are in agreement with their observations.

In the context of nociception research our finding is important because it shows that temperature increases due to mm-wave irradiation are more superficial than those based on models of multiple homogeneous layers without SGD. The temperature maxima were moved towards the EPD which is known to be populated by pain nerve fibres and heat-sensitive keratinocytes (Tillman *et al* 1995, Zylka *et al* 2005, Nolano *et al* 1999, Peier *et al* 2002). This situation is closer to a more common situation in life, that is direct contact with a hot surface, indicating that exposure to high power mm-wave irradiation should result in instantaneous acute pain responses similar to those resulting from direct contact with a hot object but without direct heating of the SC.

Only five SGD were embedded in our model due to computational requirements. It is surprising that only five glands, linearly distributed, would have a clear steady state effect on the resulting temperature distribution. It can be speculated that the effect of a two-dimensional array (e.g. 25 glands in a 5×5 array) would have an even more pronounced effect, thus moving the temperature maxima even more superficially than shown in this paper. This effect of the SGD, demonstrated here for the first time, may be involved in the hypoalgesia effect recently

reported in the literature (Radzievsky *et al* 2008). We are now actively seeking to extend our computational capabilities to improve our models and continue our studies.

5. Conclusions

In this modelling study, we present the effect of SGD on the SAR and temperature increase during skin exposure to mm-wave radiation. Our results agreed with previously published data (Feldman *et al* 2008, 2009, Walters *et al* 2000, Alekseev *et al* 2008) and suggest that SGD may act as absorption sites of mm-waves. The inclusion of SGD in the EPD resulted in a large increase in the local SAR, a moderate increase of the absolute bulk temperature and a shift of the temperature maxima towards the EPD.

Future studies will quantify the effect of a larger array and varying density of SGD on the absorption of mm-waves in the skin and the effect of thermal regulation via nearby blood vessels and skin wetness due to profuse sweating.

Acknowledgments

This work was supported by a research contract with the Office of Naval Research (N00014-09-1-0028).

We thank Schmid & Partner Engineering AG, Zurich, Switzerland for providing the SEMCAD X software for this study. We extend special gratitude to Peter Futter, Dr Esra Neufeld, Dr Pedro Crespo Valero and Maria del Mar Miñana at the SEMCAD support group for their helpful discussions and support. We thank Dr Ben Ishai for the fruitful discussions. We also extend gratitude to our collaborators, Dr William Pickard from WUSTL, Dr Michael R Cho from UIC and Dr Hemant S Thatte from HU.

This study was also supported in part by the NSF and Arkansas Science and Technology Authority grant number G1-35321-01.

References

- Alekseev S I, Radzievsky A A, Logani M K and Ziskin M C 2008 Millimeter wave dosimetry of human skin *Bioelectromagnetics* **29** 65–70
- Alekseev S I, Radzievsky A A, Szabo I and Ziskin M C 2005 Local heating of human skin by millimeter waves: effect of blood flow *Bioelectromagnetics* **26** 489–501
- Alekseev S I and Ziskin M C 2003 Local heating of human skin by millimeter waves: a kinetics study *Bioelectromagnetics* **24** 571–81
- Alekseev S I and Ziskin M C 2007 Human skin permittivity determined by millimeter wave reflection measurements *Bioelectromagnetics* **28** 331–9
- Cukierman S 2000 Proton mobilities in water and in different stereoisomers of covalently linked gramicidin A channels *Biophys. J.* **78** 1825–34
- Feldman Y, Puzenko A, Ben Ishai P, Caduff A and Agranat A J 2008 Human skin as arrays of helical antennas in the millimeter and submillimeter wave range *Phys. Rev. Lett.* **100** 128102
- Feldman Y, Puzenko A, Ben Ishai P, Caduff A, Davidovich I, Sakran F and Agranat A J 2009 The electromagnetic response of human skin in the millimetre and submillimetre wave range *Phys. Med. Biol.* **54** 3341–63
- Gabriel C, Gabriel S and Corthout E 1996a The dielectric properties of biological tissues: I. Literature survey *Phys. Med. Biol.* **41** 2231–49
- Gabriel S, Lau R W and Gabriel C 1996b The dielectric properties of biological tissues: II. Measurements in the frequency range 10 Hz to 20 GHz *Phys. Med. Biol.* **41** 2251–69
- Gabriel S, Lau R W and Gabriel C 1996c The dielectric properties of biological tissues: III. Parametric models for the dielectric spectrum of tissues *Phys. Med. Biol.* **41** 2271–93
- Holman J P 1981 *Heat Transfer* (New York: McGraw-Hill)

- Johnsen G K, Haugsnes A B, Martinsen O G and Grimnes S 2010 A new approach for an estimation of the equilibrium stratum corneum water content *Skin Res. Technol.* **16** 142–5
- Naito S, Hoshi M and Mashimo S 1997 *In vivo* dielectric analysis of free water content of biomaterials by time domain reflectometry *Anal. Biochem.* **251** 163–72
- Nolano M, Simone D A, Wendelschafer-Crabb G, Johnson T, Hazen E and Kennedy W R 1999 Topical capsaicin in humans: parallel loss of epidermal nerve fibers and pain sensation *Pain* **81** 135–45
- Peier A M *et al* 2002 A heat-sensitive TRP channel expressed in keratinocytes *Science* **296** 2046–9
- Pickard W F and Moros E G 2001 Energy deposition processes in biological tissue: nonthermal biohazards seem unlikely in the ultra-high frequency range *Bioelectromagnetics* **22** 97–105
- Pickard W F, Moros E G and Shafirstein G 2010 Electromagnetic and thermal evaluation of an applicator specialized to permit high-resolution non-perturbing optical evaluation of cells being irradiated in the W-band *Bioelectromagnetics* **31** 140–9
- Radzievsky A A, Gordiienko O V, Alekseev S, Szabo I, Cowan A and Ziskin M C 2008 Electromagnetic millimeter wave induced hypoalgesia: frequency dependence and involvement of endogenous opioids *Bioelectromagnetics* **29** 284–95
- Shafirstein G, Baumler W, Lapidoth M, Ferguson S, North P E and Waner M 2004 A new mathematical approach to the diffusion approximation theory for selective photothermolysis modeling and its implication in laser treatment of port-wine stains *Lasers Surg. Med.* **34** 335–47
- Shibasaki M, Wilson T E and Crandall C G 2006 Neural control and mechanisms of eccrine sweating during heat stress and exercise *J. Appl. Physiol.* **100** 1692–701
- Tillman D B, Treede R D, Meyer R A and Campbell J N 1995 Response of C fibre nociceptors in the anaesthetized monkey to heat stimuli: estimates of receptor depth and threshold *J. Physiol.* **485** 753–65
- Walters T J, Blick D W, Johnson L R, Adair E R and Foster K R 2000 Heating and pain sensation produced in human skin by millimeter waves: comparison to a simple thermal model *Health Phys.* **78** 259–67
- Wilke K, Martin A, Terstegen L and Biel S S 2007 A short history of sweat gland biology *Int. J. Cosmet. Sci.* **29** 169–79
- Zylka M J, Rice F L and Anderson D J 2005 Topographically distinct epidermal nociceptive circuits revealed by axonal tracers targeted to Mrgprd *Neuron* **45** 17–25